Environmental Science & Technology

pubs.acs.org/est

Article

Fungal–Mineral Interactions Modulating Intrinsic Peroxidase-like Activity of Iron Nanoparticles: Implications for the Biogeochemical Cycles of Nutrient Elements and Attenuation of Contaminants

Zhi-Lai Chi, Guang-Hui Yu,* Andreas Kappler, Cong-Qiang Liu, and Geoffrey Michael Gadd

Cite This: *Environ. Sci. Technol.* 2022, 56, 672–680

Read Online

ABSTRACT: Fungal-mediated extracellular reactive oxygen species (ROS) are essential for biogeochemical cycles of carbon, nitrogen, and contaminants in terrestrial environments. These ROS levels may be modulated by iron nanoparticles that possess intrinsic peroxidase (POD)-like activity (nanozymes). However, it remains largely undescribed how fungi modulate the POD-like activity of the iron nanoparticles with various crystallinities and crystal facets. Using well-controlled fungal–mineral cultivation experiments, here, we showed that fungi possessed a robust defect engineering strategy to modulate the POD-like activity of the attached iron minerals by decreasing the catalytic activity of poorly ordered ferrihydrite but enhancing that of well-crystallized hematite. The dynamics of POD-like activity were found to reside in molecular trade-offs between lattice oxygen and oxygen vacancies in the iron nanoparticles, which may be located in a cytoprotective fungal exoskeleton. Together, our findings unveil coupled POD-like activity and oxygen redox dynamics during fungal–mineral interactions, which increase the understanding of the catalytic mechanisms of POD-like nanozymes and microbial-mediated biogeochemical cycles of nutrient elements as well as the attenuation of contaminants in terrestrial environments.

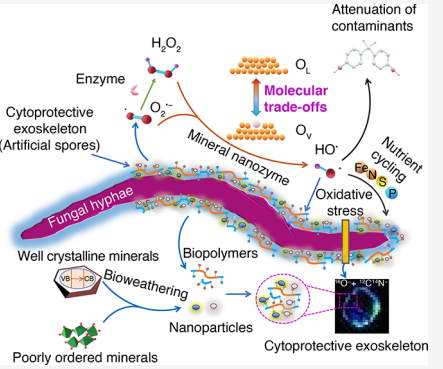

KEYWORDS: *cytoprotective exoskeleton, fungal biomineralization, Fenton reaction, iron (oxyhydr)oxide, molecular trade-offs, nanozyme, oxygen vacancy, reactive oxygen species*

INTRODUCTION

In natural environments, fungi are often interconnected to naturally occurring iron nanomaterials.[1−3] Fungal-mediated transformations of iron (Fe) minerals, i.e., fungal–mineral interactions or biomineralization, drive many biogeochemical processes in ecosystems including the transport and fate of contaminants,[4] turnover of carbon (C) and nitrogen (N),[5] and inhibition of pathogens.[6] Fungal–mineral interactions also promote organismal evolution and protect microorganisms from external stressors by the formation of an ultrathin cytoprotective exoskeleton.[7,8] As byproducts of aerobic metabolism, fungi are known to generate reactive oxygen species (ROS), i.e., extracellular superoxide ($O_2^{\bullet-}$), hydrogen peroxide (H_2O_2), and hydroxyl radical ($HO^{\bullet}$), which play a central role in these biogeochemical cycles of nutrient elements (e.g., C, N, and Fe) and contaminants.[9,10] Although ROS play a key role in cellular growth and defense systems,[11] elevated ROS levels have detrimental impacts on cells via oxidative stress and cytotoxicity,[11,12] raising the question of why and how ROS concentrations can be maintained at subtoxic levels, which is essential for fungal growth and biogeochemical cycling.

A common strategy of fungal ROS regulation is the production of various enzymes, e.g., peroxidase, catalase, or other oxidases.[12,13] However, this strategy may not only consume considerable energy but is also ineffective under "extreme" conditions, e.g., acid mine drainage systems; sites contaminated with high levels of pollutants; and at extremes of pH, alkalinity, and temperature.[14] An alternative strategy of fungal ROS regulation is to utilize attached Fe nanomaterials that are abundant in nature[1,15] and can act as biomimetic catalysts (so-called "nanozymes").[16,17] Nanozymes, i.e., nanomaterials with enzyme-like activities, are superior to natural enzymes in several aspects, such as their high stability, large surface areas available for bioconjugation, and multifunctionality.[18] These biological–nanoparticle interactions may reflect perfectly the unique ecological, biological, and morphological plasticity of fungi in response to extreme environments.[19] Based on their distinct properties of particle size, shape, specific surface area, and crystallinity, biocompatible Fe

Received: September 29, 2021
Revised: November 28, 2021
Accepted: December 1, 2021
Published: December 14, 2021

minerals, ranging from poorly ordered ferrihydrite to well-crystalline hematite,[20,21] are predicted to possess a distinct catalytic activity and thus mitigate differential oxidative stress on fungi. However, the mechanisms by which fungi modulate the catalytic activity of attached iron nanomaterials, of varied crystallinity and crystal facets, for the purpose of maintaining subtoxic ROS levels and nutrient acquisition, remain largely undescribed. This lack of knowledge limits our understanding of fungal- and mineral-mediated biogeochemical processes in terrestrial ecosystems.

Because of the broad applications of Fe (oxyhydr)oxide mineral nanozymes (mainly as peroxidase (POD)-like activity), ranging from biosensors, biomedical diagnosis to environmental remediation, their catalytic mechanisms have gained extensive attention.[22−24] A growing body of evidence has revealed that nanoparticle surfaces[25−27] rather than the classical Fenton catalysis[23] are responsible for the catalytic activity of Fe (oxyhydr)oxide mineral nanozymes. It is known that the catalytic activity occurring on nanoparticle surfaces is ∼50-fold more effective in driving $HO^{\bullet}$ production than dissolved ferric iron ions,[28] probably attributable to the higher catalytic reactivity of ferrous ions bound on mineral facets than that of ferric iron ions.[29] These mineral nanoparticles are usually adsorbed to negatively charged, bioactive molecules in the cell wall and extracellular materials exuded by fungi,[30] creating a suitable environment to form a cytoprotective exoskeleton.[17,31] To date, the activity descriptors and the location of POD-like nanozymes remain unclear.

In this research, we examined the dynamics of iron mineral nanozymes, with various crystallinities and crystal facets, when interacting with a fungus. We investigated the molecular trade-offs between lattice oxygen (O_L) and oxygen vacancy sites (O_V) that may drive the POD-like activity of iron (oxyhydr)-oxide mineral nanozymes under physiological conditions. To this end, we performed a series of well-controlled fungal−mineral cultivation experiments by selecting *Trichoderma guizhouense* NJAU 4742 as the model fungus and a diverse set of Fe(III) (oxyhydr)oxides as model iron minerals due to their ubiquity in the terrestrial environment and their strong catalytic activities.[1,32] The Fe minerals examined included poorly ordered ferrihydrite, as well as crystalline goethite and hematite, and also hematite nanoplates with the (001) plane as the dominant facet (named as hematite (001) thereafter)[29] and hematite nanocubes equally enclosed by (012), (102), and (−112) planes (named as hematite (012) thereafter).[33] We hypothesized that fungi can drive Fe mineral nanozyme activity by modulating the Fe mineral nanoparticles with surface deficiency (also called defect engineering[34]). Because of missing or dislocated atoms (e.g., O in this study), these defect sites locally break the regular periodic arrangement of atoms in the crystalline structures.[35] During this defect engineering, O_L may be removed by fungal activity from anion sites leaving behind surface defects (e.g., O_V). Thus, the molecular trade-offs between O_L and O_V on minerals result in the introduction of oxygen defects that may serve as reactive centers to drive intrinsic nanozyme activity, owing to their lower adsorption energies of H_2O_2 and desorption energy of $HO^{\bullet}$.[34] During these engineered defects, fungi regulate POD-like activity of iron (oxyhydr)oxide mineral nanozymes that catalyze H_2O_2 into $HO^{\bullet}$ and form the oxidized substrates,[23] thus changing ROS levels around the cell.

MATERIALS AND METHODS

Iron Mineral Preparation. Iron (oxyhydr)oxide minerals with various crystallinity and crystal facets, including ferrihydrite, goethite, hematite, hematite (001), and hematite (012), were selected in this study. All chemicals were analytical reagents and purchased from J&K Scientific, Beijing, China. In brief, ferrihydrite was prepared by adding 330 mL of 1 M KOH to 500 mL of 0.05 M $Fe(NO_3)_3{\cdot}9H_2O$.[37] Goethite was prepared by mixing 100 mL of 1 M $Fe(NO_3)_3{\cdot}9H_2O$ with 180 mL of 5 M KOH, and then aging (60 h, 70 °C). Hematite was synthesized by mixing 2 L of 0.04 M $Fe(NO_3)_3{\cdot}9H_2O$ with 0.002 M HNO_3 (98 °C) and then aging (7 days, 98 °C). Synthesis of hematite (001) was done as follows:[29] 1.35 g of CH_3COONa and 0.5 g of $FeCl_3{\cdot}6H_2O$ were first dissolved in 14.5 mL of poly(ethylene glycol) (PEG), stirred vigorously (30 min), transferred into a Teflon-lined autoclave (20.0 mL), and then heated at 200 °C for 12 h in an electronic oven. Preparation of hematite (012) was done as follows:[29,33] 1.62 g of $FeCl_3{\cdot}6H_2O$ was first dissolved in 50 mL of 0.04 mol L^{-1} cetyltrimethylammonium bromide (CTAB) aqueous solution. Then, the whole mixture was stirred for 30 min and transferred into a 20 mL Teflon-lined stainless-steel autoclave, sealed, and maintained at 120 °C for 32 h.

The ionic impurities in the five suspensions were removed by dialyzing with deionized water for 3 days. The pellets were then vacuum freeze-dried, stored in a desiccator, and used for cultivation experiments within 1 week. The Brunauer−Emmett−Teller (BET) surface areas of five Fe minerals were determined as follows (units: $m^2\ g^{-1}$): 280 for ferrihydrite, 25 for goethite, 38 for hematite, 31 for hematite (001), and 0.4 for hematite (012).

Fungal−Mineral Cultivation Experiments. *T. guizhouense* NJAU 4742[6] was used as the experimental fungus. All cultivation experiments were performed at 28 °C in the dark. For fungal growth, the following medium was used (per L): 20 g of glucose, 100 mg of urea, 100 mg of yeast extract, 1500 mg of KH_2PO_4, 1400 mg of $(NH_4)_2SO_4$, 400 mg of $MgSO_4{\cdot}7H_2O$, 100 mg of $CaCl_2{\cdot}2H_2O$, 5 mg of $FeSO_4{\cdot}7H_2O$, 2.5 mg of $ZnSO_4{\cdot}7H_2O$, 1.8 mg of $MnSO_4{\cdot}H_2O$, 5 mg of $CoCl_2$, and 600 mg of NaCl. The cultivation experiments were initiated by adding 0.1% (w/v) iron mineral to the liquid medium that was inoculated with10^4 mL^{-1} of *T. guizhouense* conidia and then incubated in a shaking incubator (170 rpm).

POD-like Nanozyme Activity Assay. POD-like nanozyme activity assays were carried out using 3,3′,5,5′-tetramethylbenzidine (TMB) solution (10 μL of 5 mg mL^{-1}) in dimethyl sulfoxide (DMSO) as the substrate in 2 mL tubes. Each tube contained 1 mg of Fe mineral nanoparticles in the test TMB solution (1 mL) in 0.2 M NaAc-HAc buffer (pH 3.6). After H_2O_2 input (to a final concentration of 50 mM), a blue color was observed at 28 °C and measured at 652 nm every 15 s for up to 10 min using a SpectraMax M5 spectrophotometer (Molecular Devices, Sunnyvale, CA). The control was set without addition of H_2O_2 or TMB solution. The POD-like activity (units) of Fe (oxyhydr)oxide mineral nanozymes was calculated as follows[36]

$$b_{\text{nanozyme}} = V/(\varepsilon \times l) \times (\Delta A/\Delta t) \quad (1)$$

where b_{nanozyme} is the nanozyme activity expressed in catalytic units; V is the total reaction volume (μL); ε is the molar absorption coefficient of the substrate; l is the path length of

https://doi.org/10.1021/acs.est.1c06596
Environ. Sci. Technol. 2022, 56, 672−680

light (cm); and $\Delta A/\Delta t$ is the initial rate of change in absorbance at 652 nm in min^{-1}.

High-Resolution X-ray Photoelectron Spectroscopy (XPS) Analyses. XPS analyses were conducted using a PHI 5000 Versa Probe (UlVAC-PHI, Japan) spectrometer equipped with a monochromatic Al X-ray source (1486.6 eV). For achieving the absolute binding energy, the C 1s signal (284.8 eV) was used as an internal reference. The surface charge was balanced using a flood gun at 6 eV. The base pressure of the spectrometer was 6.7×10^{-10} Torr. For wide-scan spectra, an energy range of 0−1100 eV was used with a step size of 1 eV and a pass energy of 80 eV. High-resolution XPS spectra were collected with a step size of 0.06 eV and a pass energy of 40 eV. The energy precision was 0.06 eV. The high-resolution O 1s and C 1s XPS spectra were fitted using the CasaXPS software.[38]

Nanoscale Secondary Ion Mass Spectrometry (Nano-SIMS) Analyses. Fungal−mineral cultivated samples were fixed, dehydrated, embedded, and cut into 1 μm thick sections using a Diatome diamond knife (Leica UCT ultramicrotome). The samples were then gold-coated and examined using scanning electron microscopy (SEM) (Zeiss EVO18 scanning electron microscope) with a 20 kV accelerating potential. The samples were next analyzed using a NanoSIMS 50L (Cameca, Gennevilliers, France) instrument at the School of Earth System Science, Tianjin University, China. Prior to NanoSIMS analysis, a gold coating layer (~15 nm) was first pre-sputtered using a high primary beam current (pre-sputtering). Secondary ions of $^{12}C^{14}N^-$ and $^{16}O^-$ were collected by electron multipliers.[26] The NanoSIMS image sizes were 25×25 μm^2. The $^{12}C^{14}N^-$ ion was interpreted as representing fungal biomass or bioactive molecules, while $^{16}O^-$ ion was interpreted as mineral O, respectively.[26] The charging effect was compensated for using an electron flood gun. Thickness measurements of the cytoprotective exoskeleton, based on the line profile analysis from NanoSIMS images, were conducted using ImageJ (version 1.45) combined with the OpenMIMS plugin (http://www.nrims.hms.harvard.edu/NRIMS_ImageJ.php).

Transmission Electron Microscopy (TEM) and Physicochemical Analyses. To observe the morphology of mineral particles, samples were dispersed in ethanol and then dropped onto C-coated copper grids. After being air-dried, the samples were observed by a TEM (JEM-1400 PLUS) operating at an acceleration voltage of 120 keV. The BET surface areas of Fe minerals were obtained from N adsorption isotherms obtained using a Micromeritics Tristar3000 instrument.[29] Extracellular $O_2^{\bullet-}$ and H_2O_2 were detected using specific stains.[10] *T. guizhouense* colonies on potato dextrose agar (PDA) plates were flooded with nitroblue tetrazolium (NBT) chloride and 3,3′-diaminobenzidine (DAB) for $O_2^{\bullet-}$ and H_2O_2, respectively. The NBT assay was composed of NBT chloride (2.5 mM, Sigma, St. Louis, MO) and 3-(N-morpholino) propanesulfonate NaOH (5 mM, pH 7.6). The plates were first incubated with the stains in the dark and then imaged using a stereomicroscope (Leica DM 5000B, Leica Microsystems, Germany). In this assay, blue and brown precipitates indicate the presence of $O_2^{\bullet-}$ and H_2O_2, respectively.

Statistical Analyses. Significant differences were determined by Duncan's multiple range test at $p < 0.05$. One-way analysis of variance (ANOVA) was used to assess the data (means ± SD, $n = 3$) using IBM SPSS statistics 20.0.

RESULTS AND DISCUSSION

Contrasting POD-like Activity of Fe (Oxyhydr)oxide Mineral Nanozyme Responses to Fungal Growth. Predictably, the morphology (Figure 1A) and crystalline

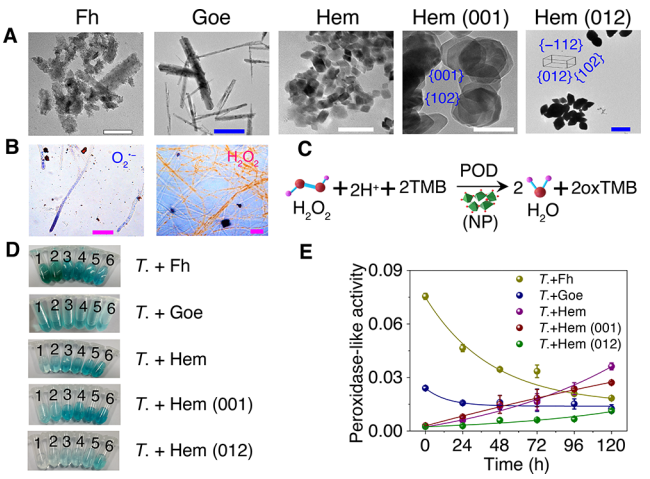

Figure 1. Morphology and POD-like activity of Fe mineral nanozymes during fungal−mineral interactions. (A) TEM images of original Fe mineral nanozymes. Scale bars represent 100 nm (white) and 1 μm (blue), respectively. (B) Location of $O_2^{\bullet-}$ (blue) and H_2O_2 (pink) in fungal hyphae shown by staining. Scale bar, 10 μm. (C) Catalytic reaction of POD mimics (i.e., nanozymes) in the presence of H_2O_2 (electron acceptor) with colorless 3,3′,5,5′-tetramethylbenzidine (TMB) to form blue oxidized TMB (oxTMB). NP, iron mineral nanoparticles. (D) Photograph of colorimetric reaction after 10 min incubation of Fe mineral nanozymes (1 mg) with H_2O_2 (50 mM) + TMB (10 μL, 5 mg mL^{-1}) in pH 3.6 buffer. Tubes 1−6 represent Fe mineral nanozymes at the cultivation times of 0, 24, 48, 72, 96, and 120 h, respectively. (E) Changes in the POD-like activity of Fe mineral nanozymes with cultivation time. Data are mean ± SD (n = 3). T.+Fh, *T. guizhouense* plus ferrihydrite; T.+Goe, *T. guizhouense* plus goethite; T.+Hem, *T. guizhouense* plus hematite; T.+Hem (001), *T. guizhouense* plus hematite (001); T.+Hem (012), *T. guizhouense* plus hematite (012); POD, peroxidase.

structures (Figure S1) of five selected Fe (oxyhydr)oxide mineral nanozymes were distinct. TEM and X-ray diffraction (XRD) revealed that ferrihydrite was two-line ferrihydrite, poorly crystalline, and aggregated as nanosized particles, while goethite and hematite were well crystallized and possessed a larger particle size than ferrihydrite. Although all of the hematites possessed the same X-ray diffraction pattern (Figure S1A), their morphologies were clearly different, i.e., hematite of hexagonal shape, hematite (001) with a dominant (001) facet, and hematite (012) composed of (012), (102), and (−112) planes (Figure 1A). After 120 h cultivation, the crystalline structures of goethite, hematite, hematite (001), and hematite (012) remained stable, which may be attributable to surface-sorbed organic carbon that prevents these minerals from undergoing phase transformation[39] (Table S1). However, the poorly crystalline structure of ferrihydrite changed to a large extent (Figure S1B), i.e., with the presence of several prominent peaks at 9.0, 12.2, 19.2, 32.1, and 35.3 Å, suggesting an unstable structure of the poorly ordered ferrihydrite compared to well-crystallized goethite and hematite during fungal cultivation experiments.

NBT and DAB staining[10] confirmed hotspots with concentrated $O_2^{\bullet-}$ on hyphae as well as a more diffuse

https://doi.org/10.1021/acs.est.1c06596
Environ. Sci. Technol. 2022, 56, 672−680

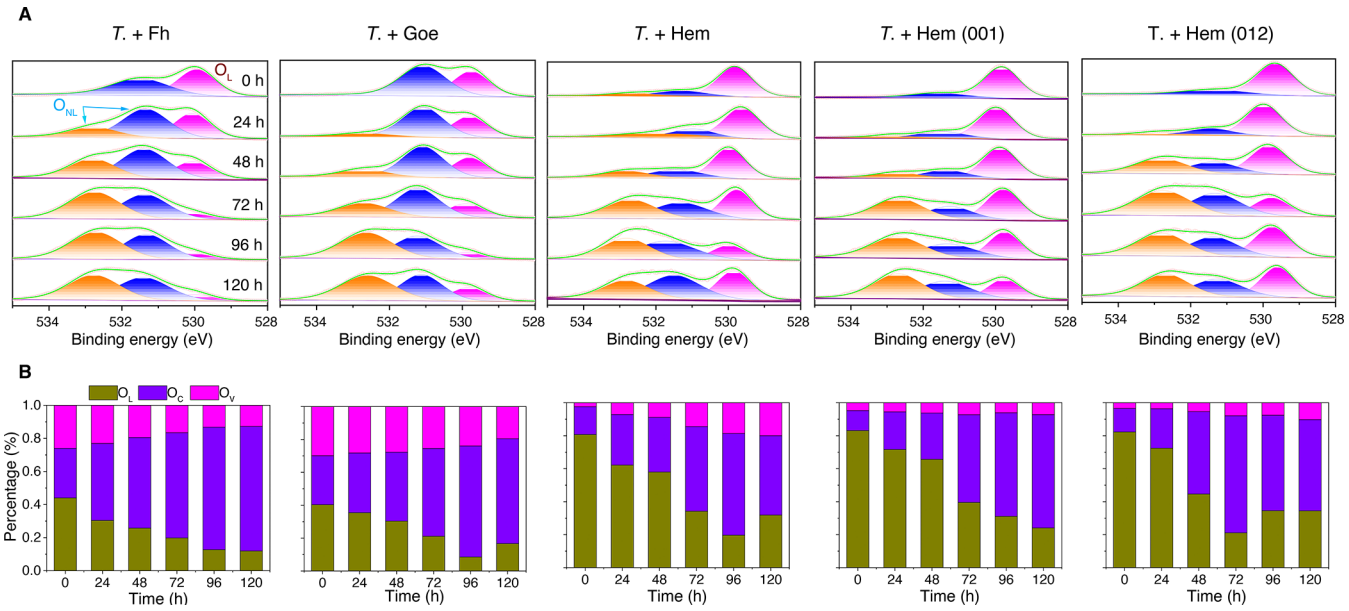

Figure 2. Molecular trade-offs between O_L and O_V during fungal−mineral interactions. (A) O 1s core-level XPS spectra of Fe mineral nanozymes. (B) Relative abundance of O_L, O_V, and O_C. In the O 1s spectrum: the cyan peak located at ∼529.7 eV is assigned to the lattice oxygen (O_L) bonded to cations, while the blue and orange peaks centered at around 531.6 and 532.5 eV are referred to the nonlattice O (O_{NL}) or adsorbed O species, mainly composed of O vacancy (O_V) and carbon−oxygen groups (O_C). Specifically, O_V, occupied by hydroxyl species (OH^-), and its deprotonated form O^{2-}, exhibit a strong catalytic capacity, while O_C, occupied by carbon−oxygen groups (C−O and C−O═C), is suggested to have reduced catalytic capacity.[38,44] T.+Fh, *T. guizhouense* plus ferrihydrite experiment; T.+Goe, *T. guizhouense* plus goethite; T.+Hem, *T. guizhouense* plus hematite; T.+Hem (001), *T. guizhouense* plus hematite (001); T.+Hem (012), *T. guizhouense* plus hematite (012).

distribution of H_2O_2 along the hyphae after 120 h cultivation of the fungus in the presence of ferrihydrite (Figure 1B), which was in agreement with our previous observations for fungal + hematite cultivation.[26,40] Fungal activity (Figure S2) created an acidic environment (Figure S2A), initiating the decay of H_2O_2 in the presence of Fe mineral nanoparticles through POD-like nanozyme activity[22] (Figure 1C). During fungal−mineral cultivation, fungal biomass increased gradually with cultivation time, in line with an increase in biological activity[41] (Figure S3), implying that the fungus was bioactive over the entire cultivation period. Intriguingly, the POD-like activity of Fe mineral nanozymes was affected differentially by growth of the fungus (Figure 1D,E). Specifically, the colorimetric signal of poorly ordered ferrihydrite gradually became more intense with cultivation time; conversely, the colorimetric signal of well-crystallized hematite, hematite (001), and hematite (012) decreased in intensity with cultivation time (Figure 1D). The colorimetric signal in the presence of goethite changed only slightly. These observations suggested that over 120 h cultivation, POD-like activity decreased gradually for poorly ordered ferrihydrite but markedly increased for well-crystallized hematite.

By calculating the POD-like activity of Fe mineral nanozymes, it was evident that at the initial time point (0 h), ferrihydrite had the highest POD-like activity (0.075), which was ∼3 times and 37 times higher than those of goethite (0.024) and hematite (0.002). Furthermore, the activity of the hematite (001) facet corresponded to ∼80% of the POD-like activity from hematite. Compared to ferrhydrite and hematite, the POD-like activity of goethite only slightly decreased during 120 h cultivation. Therefore, during fungal−mineral interactions, the POD-like activity of ferrihydrite and goethite dropped over 3 and 1 times, respectively. In contrast, the POD-like activity of hematite increased aprroximately 17 times. Together, these results provide the first evidence that fungal growth has a contrasting effect on POD-like activity of the different Fe (oxyhydr)oxide mineral nanozymes, i.e., reducing the catalytic activity of poorly crystalline ferrihydrite but enhancing the catalytic activity of well-crystallized hematite.

Linking Fe Mineral Nanozyme Activity to the Molecular Trade-Offs between Lattice Oxygen and Oxygen Vacancy Sites. Iron cations are known to catalyze H_2O_2 to $HO^\bullet$ through Fenton catalysis.[15] However, the absence of dissolved Fe and solid-phase Fe(II) during the initial 24 h cultivation and the disproportionate changes in dissolved Fe and solid Fe(II) with POD-like activity (Figure S2B,C) implied that Fe(II) ions in our systems were not responsible for the changed POD-like activity. This observation was consistent with a previous report, which found that catalytic reactions on the mineral nanoparticle surface were several times more effective than dissolved Fenton agents.[42] Furthermore, high-resolution XPS spectroscopy, a near-surface sensitive technique,[43] was used to gain insight into changes in the molecular structures of Fe and O in the iron(III) (oxyhydr)oxides. Wide-scan XPS spectra of the Fe minerals indicated the presence of Fe, O, and C (Figure S4A). Changes in the peak intensities of surface Fe (Figure S5A,B) were obviously more pronounced than those for bulk Fe (Figure S5C), and almost no shift of the Fe local coordination position during fungal−mineral interactions was observed. Combined with Fe chemistry in solution (Figure S5B,C), these spectroscopic features suggest that part of the Fe is transferred from the minerals into solution and that surface Fe structures (Figure S5) may not dominate the changed POD-like activity of Fe mineral nanozymes (Figure 1D,E).

Surface O anions of mineral nanozymes are a significant redox partner for transition-metal (TM) cations (e.g., Fe in

https://doi.org/10.1021/acs.est.1c06596
Environ. Sci. Technol. 2022, 56, 672−680

this study) due to the strong hybridization between TM 3d and O 2p electronic states.[43] In stark contrast to the stable Fe spectra over time (Figure S5), O 1s core-level XPS spectra showed that the chemical states of O atoms from Fe mineral nanozymes had a dramatic change. One peak centered at ~529.7 eV is assigned to the O_L bonded to Fe, whereas the others centered at ~531.6 and ~532.5 eV are attributed to adsorbed O species or nonlattice O (O_{NL}), mainly composed of O_V (i.e., occupied by hydroxyl species (OH^-) and its deprotonated form (O^{2-}) and carbon−oxygen functional groups (O_C, i.e., C−O and C−O═C).[44] Based on the integrated area of Gaussian-resolved peaks, the O_{NL} percentage (i.e., O_V + O_C) for all of the examined Fe mineral nanozymes increased with cultivation time (Figure 2). Changes in O_{NL} and POD-like activity reveal that O_{NL}, the mixture of vacant oxygen (O_V) and carbon−oxygen functional groups (O_C), cannot be used as the determinant of catalytic activity in Fe mineral nanozymes.

The catalytic activity of mineral nanozymes is attributed to the ability of Fe (oxyhydr)oxides to undergo rapid redox cycles by releasing and storing O, where O_V sites chiefly contribute to the catalytic activity, owing to O_C being short of a prominent catalytic capacity.[38,44] To disentangle the relative contribution of O_V from the total O_{NL}, we reevaluated the proportion of surface O_V (i.e., $c(O_V)$) by combining with C 1s core-level XPS spectra (Figure S4B and Tables S1 and S2), based on eq 2[38]

$$c(O_V) = c_{oxygen} \times c(\text{adsorbed O}) - c_{carbon} \times [c(C-O) + 2 \times c(O-C=O)] \quad (2)$$

Note that eq 2 is used to approximate the content of adsorbed hydroxyl species (OH^- and its deprotonated form O^{2-}) from the difference between total adsorbed O species (OH^-, O^{2-}, C−O, O−C═O) and carbon−oxygen groups (C−O, O−C═O).[38,44] Remarkably, the percentage of V_O exhibited a pronounced positive and linear relationship ($R > 0.6$, $p < 0.01$, $n = 18$) with POD-like activity for all of the examined Fe mineral nanozymes (Figure 3), strongly revealing that surface OH^- and O^{2-} are the key regulators of POD-like activity in Fe mineral nanozymes. The presence of V_O was further confirmed by Fe K-edge extended X-ray absorption fine structure (EXAFS) spectra (Figure S5C), which showed a pronounced intensity decrease for ferrihydrite and goethite cultivations but an increase for hematite, hematite (001), and hematite (012) was observed at 1.7 $Å^{-1}$ with time, which matched with the changes in Fe−O bonds and thus the existence of V_O in the bulk minerals.[45] Our spectral evidence suggested that fungal activity causes Fe migration from mineral nanoparticles (Figure S5) to solution (Figure S2B,C), leaving spaces with O-deficient interfaces, and thus O atoms on the Fe mineral lattice (Fe−O) easily escape to create O_V (Fe−O + Fe−O → 2Fe−O_V + O_2).[46] The O-deficient interfaces and the formed O_V sites were evidenced by an increase in surface hydroxyl species (OH^-) at around 532.5 eV (Figure 2) and a decrease in Fe−O bonds at 1.7 $Å^{-1}$ (Figure S5C). The O_V sites are shown to be mainly occupied by adsorbed hydroxyl species.[44,46] In summary, we show unexpected and exciting findings that fungi modulate the defect engineering, i.e., the molecular trade-offs between O_L and O_V in mineral nanoparticles during fungal−mineral interactions, probably with benefits in regulating Fe mineral nanozyme activity and maintaining ROS concentrations at subtoxic levels.

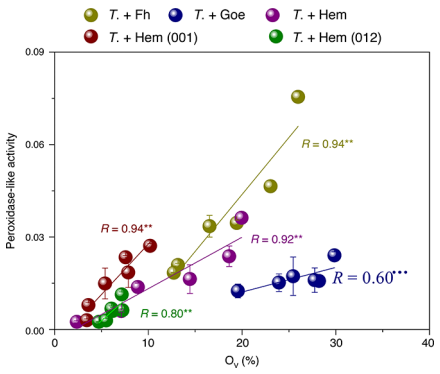

Figure 3. Relationship between O_V and POD-like activity. T.+Fh, *T. guizhouense* plus ferrihydrite; T.+Goe, *T. guizhouense* plus goethite; T.+Hem, *T. guizhouense* plus hematite; T.+Hem (001), *T. guizhouense* plus hematite (001); T.+Hem (012), *T. guizhouense* plus hematite (012); O_V, oxygen vacancy. POD, peroxidase. Data are mean ± SD ($n = 3$). **$p < 0.01$.

High-Resolution Detection of Fungal Nanozyme Catalytic Sites. Fungus-mediated catalytic reactions must mainly occur at fungal surfaces because first, fungal exudated $O_2^{\bullet-}$ does not diffuse far from its formation site[47] and second, $HO^{\bullet}$ has a very short half-life (approximately several nanoseconds).[48] To localize the catalytic sites of the Fe mineral nanozymes on fungal hyphae, NanoSIMS imaging was used to provide high spatial resolution (down to 50 nm[49]) characterization of both mineral O anions and organic substances. After 120 h cultivation, fungal−mineral cultivated samples were fixed, embedded in epoxy resin, and cut into transverse sections (1 μm thick) (Figure 4A). SEM images clearly showed the position of fungal hyphae, while NanoSIMS images further indicated that the hyphae were surrounded by a layer that contained mineral O ($^{16}O^-$) and organic substances ($^{12}C^{14}N^-$) (Figure 4A), consistent with observations of the whole hyphae, which exclude possible interference from the epoxy resin used for embedding (Figure S6). Furthermore, synchrotron radiation-based scanning transmission X-ray microscopy (STXM) images also supported the presence of a heterogeneous mineral O layer on the examined hyphae (Figure S7). These observations are compatible with previous reports suggesting that the cytoprotective exoskeleton can act as a "cell-in-shell" structure.[50−52] In nature, hard cytoprotective exoskeletons are commonly used to protect microbial soft tissues from environmental stress.[8] To determine the thickness of the cytoprotective exoskeleton on the hyphae, a region of interest (ROI) analysis[53] was conducted. The results from ROI analysis revealed that the thickness of the cytoprotective exoskeleton was ~0.1 to 0.6 μm (Figure 4B). These observations demonstrate that the POD-like activity of Fe mineral nanozymes may reside mainly in this thin cytoprotective exoskeleton, which provides a similar protective barrier analogous to fungal spores.

Proposed Catalytic Reactions in the Fungal Cytoprotective Exoskeleton. Although cytoprotective exoskeleton coatings have been demonstrated to form on taxonomically and ecologically diverse bacteria,[52] yeast cells,[50,54] and filamentous fungi,[55] this study provides the first evidence that links POD-like activity in the cytoprotective exoskeleton to the molecular trade-offs between O_L and O_V in the Fe mineral nanoparticles. Fungal biomineralization can alter the

https://doi.org/10.1021/acs.est.1c06596
Environ. Sci. Technol. 2022, 56, 672−680

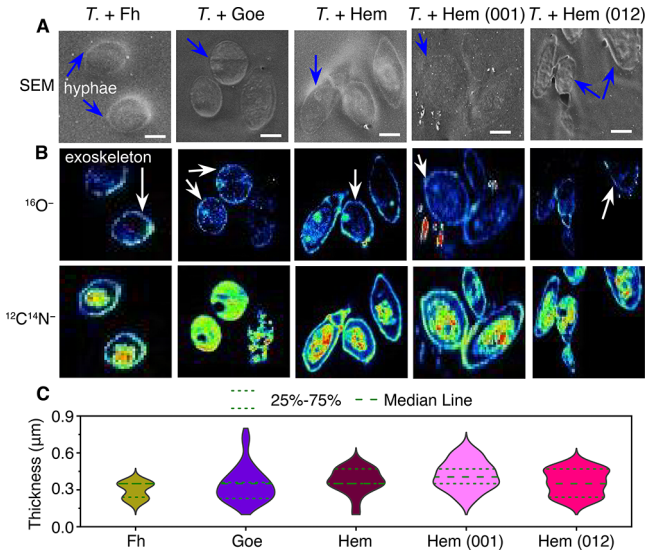

Figure 4. Cross-sectional (1 μm thickness) observation of the fungal cytoprotective exoskeleton on a single hypha after 120 h cultivation. (A) Correlative SEM and NanoSIMS images. (B) Thickness of cytoprotective exoskeleton based on the line profile analysis from NanoSIMS images. Secondary ions for $^{16}O^-$ and $^{12}C^{14}N^-$ indicate the presence of mineral O and fungal hyphae, respectively. Blue and white arrows indicate the presence of fungal hyphae and cytoprotective exoskeleton, respectively. "*n*" in (b) is the number of hyphae. Scale bar = 2 μm. T.+Fh, *T. guizhouense* plus ferrihydrite; T.+Goe, *T. guizhouense* plus goethite; T.+Hem, *T. guizhouense* plus hematite; T. +Hem (001), *T. guizhouense* plus hematite (001); T.+Hem (012), *T. guizhouense* plus hematite (012); SEM, scanning electron microscopy; NanoSIMS, nanoscale secondary ion mass spectrometry.

surface properties (Figures 2, S4, and S5) of Fe minerals through Fe(III) reduction (Figure S2B), cation migration (Figure S2C), and co-precipitation (Figures 4 and 5) processes.[2,26,40] These processes break the regular periodic arrangement of atoms (e.g., Fe and O) in the crystalline structures (Figures 2 and S5) and leave behind surface defect sites (Figure S5).[35] The surface defect sites are reported to serve as reactive centers to drive intrinsic nanozyme activity.[34] We accordingly propose that during fungal−mineral interactions, the fungal cell wall and exudated extracellular polymeric substances (EPS, Figure S3)[30] create abundant nucleation sites, which retain Fe ions and mineral nanoparticles (Figure 5), and that this intimate relationship between metals and biopolymers further promotes the rapid formation of a cytoprotective exoskeleton (Figure 4).[17,31] The cytoprotective exoskeleton is capable of initiating complex, artificial biochemical cascades (including biocatalysis) on the cells.[16,17]

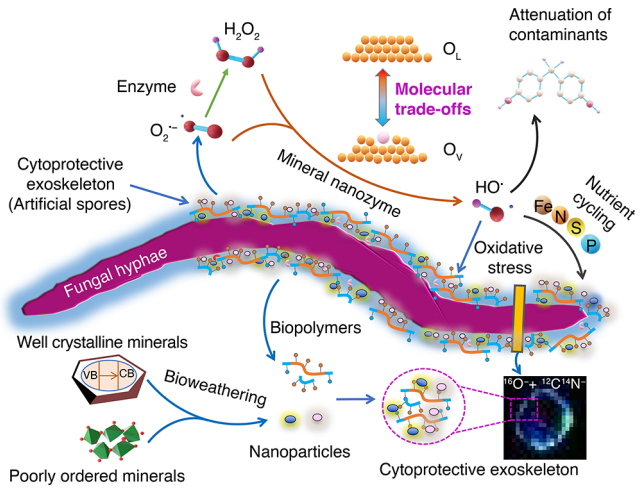

Figure 5. Schematic of fungal-mediated molecular trade-offs between lattice oxygen and oxygen vacancy sites controlling intrinsic peroxidase-like activity of iron (oxyhydr)oxide mineral nanoparticles.

Furthermore, the catalytic reactions occurring in the fungal cytoprotective exoskeleton may include multiple steps (Figure 5). First, H_2O_2 excreted by the fungus (Figure 1B) may react with Fe minerals and produces surface Fe(II) (Figure S3B) and peroxide radicals through Fenton-like reactions.[56] On the mineral surface, Fe minerals are hydrated, and in a first step, the adsorbed H_2O can be exchanged with exuded H_2O_2, which is thermodynamically favorable ($\Delta G^\circ < 0$).[57] Second, the dissociation of H_2O_2 leads to Fe(II) oxidation with hydroxyl species OH^- and $HO^\bullet$ ligands. Hydroxyl species on the mineral surfaces (Table S1) can enhance V_O production (Figures 2 and S5C) and further produce adsorption sites for OH^- and H_2O (Figure 2).[44] As a result, surface-hydroxylated minerals yield more $HO^\bullet$. Finally, a release of $HO^\bullet$ radicals from these species into solution occurs, but this may be undetectable owing to its short half-life.[57] The $HO^\bullet$ radicals usually react with substrates on sites (Figure 1C−E), whereas the estimated diffusion distance of H_2O_2 is about 1.5 mm.[48] Thus, we surmise that fungal exuded H_2O_2 can diffuse in the fungal cytoprotective exoskeleton (Figure 4) and then react with Fe mineral nanozymes (Figure 1C−E). As a sink of $HO^\bullet$ radicals, the EPS matrix (Figures 4 and S3)[30] on the cell surface will protect the fungus from being exposed to its own ROS. Because the catalytic behavior of Fe mineral nanozymes (Figure 1D,E) strongly depends on their surface area, crystal morphology, and crystalline structure,[24,58] poorly ordered ferrihydrite had a higher (3−30 times) catalytic activity than well-crystallized goethite and hematite (Figure 1D,E).

Environmental Implications. Using a combination of classic POD colorimetric reactions, high-resolution XPS spectra, and NanoSIMS images, our findings unambiguously reveal key traits that determine the POD-like activity of Fe mineral nanoparticles during fungal−mineral interactions. Specifically, fungi drive POD-like activity by modulating the molecular trade-offs between O_L and O_V in Fe(III) (oxyhydr)-oxide mineral nanoparticles, which might occur mainly at a thin (hundreds of nanometer thickness) cytoprotective fungal exoskeleton. In particular, our findings indicate varying effects for different mineral facets of the same (hematite) mineral on POD-like activity, pointing to the importance of further exploration of structure−activity relationships[59,60] that influence the POD-like activity of mineral nanozymes.

Although large amounts of nutrients can be closely associated with minerals, i.e., coexisting as mineral−organo associations in terrrestrial environments,[21,61] fungi have been demonstrated to possess the ability to access carbon and other nutrient elements (e.g., nitrogen, phosphorus, and iron) from mineral-associated organic matters through regulation of ROS levels.[5,26,40,61−64] In this study, our findings suggest that fungal regulation of the ROS level may be mainly located at their cytoprotective exoskeleton layers, and therefore play a more important role in the biogeochemical cycling of C, N, P, and Fe than has been previously appreciated (e.g., extracellular enzymes and carbon-based metabolism[65]). This emphasizes that the fungal cytoprotective exoskeleton acts as an "artificial

https://doi.org/10.1021/acs.est.1c06596
Environ. Sci. Technol. 2022, 56, 672−680

cell coating"[17] to enable new or augmented biological functions, e.g., preserving enzymatic activity[66] and cell viability,[67] as well as enhancing extracellular electron transfer.[68,69] In summary, the consequences of our findings regarding the molecular trade-offs between oxygen anions improve our understanding of the role of mineral nanomaterials in fungal-mediated biogeochemical cycles of carbon and other elements in terrestrial environments.

Fungi have acquired many of their biofunctionalities over ~1.0 billion years of evolution,[70] but fungal evolution in degrading organic pollutants lags behind the rapid increase of synthetic organic pollutants in the new human-influenced geological epoch, the Anthropocene.[71] Our findings suggest that fungi may evolve in successfully coping with organic pollutants by interacting with surrounding redox-active Fe minerals and forming cytoprotective exoskeleton layers. These cytoprotective exoskeleton layers not only prevent the intimate contact between cells and pollutants but also improve the degradation efficiency of organic pollutants by producing nonselective strong oxidant $HO^{\bullet}$ radicals.[8,17,50] More broadly, given that teragram (Tg)-level abundance of mineral nanoparticles[1] and ~12 Gt (gigaton ton, 10^9 ton) C of fungal biomass[72,73] are present in terrestrial ecosystems, the current research has prompted us to further explore fungal−mineral interactions that produce $HO^{\bullet}$ radicals, which have multiple environmental and ecological implications, including nutrient acquisition[62] and the potential *in situ* degradation of organic contaminants.[74] Since fungi constitute a vast kingdom of ~2 to 6 million or more species,[19] future studies are warranted to explore whether modulation of molecular trade-offs between oxygen anions in Fe minerals is a widespread fungal property.

■ ASSOCIATED CONTENT

Supporting Information

The Supporting Information is available free of charge at https://pubs.acs.org/doi/10.1021/acs.est.1c06596.

Typical XRD patterns of Fe mineral nanozymes; changes in pH, Fe(II) and dissolved Fe, fungal biomass, and activity; wide-scan and C 1s core-level XPS spectra of Fe minerals; Fe 2p core-level XPS, Fe L-edge XANES, and Fe K-edge EXAFS spectra; location of mineral O, Fe (oxyhydr)oxides and fungal biomass; STXM; atomic concentration; and proportion of C−H, C−O, and O−C═O in total carbon (PDF)

■ AUTHOR INFORMATION

Corresponding Author

Guang-Hui Yu − *Institute of Surface-Earth System Science, School of Earth System Science, Tianjin Key Laboratory of Earth Critical Zone Science and Sustainable Development in Bohai Rim, Tianjin University, Tianjin 300072, China;* orcid.org/0000-0002-5699-779X; Phone: +86-22-27405053; Email: yuguanghui@tju.edu.cn; Fax: +86-22-27405051

Authors

Zhi-Lai Chi − *Institute of Surface-Earth System Science, School of Earth System Science, Tianjin Key Laboratory of Earth Critical Zone Science and Sustainable Development in Bohai Rim, Tianjin University, Tianjin 300072, China; Jiangsu Provincial Key Laboratory for Organic Solid Waste Utilization, College of Resource & Environmental Sciences, Nanjing Agricultural University, Nanjing 210095, China*

Andreas Kappler − *Geomicrobiology, Centre for Applied Geosciences, University of Tübingen, Tübingen 72076, Germany;* orcid.org/0000-0002-3558-9500

Cong-Qiang Liu − *Institute of Surface-Earth System Science, School of Earth System Science, Tianjin Key Laboratory of Earth Critical Zone Science and Sustainable Development in Bohai Rim, Tianjin University, Tianjin 300072, China*

Geoffrey Michael Gadd − *Geomicrobiology Group, School of Life Sciences, University of Dundee, Dundee DD1 5EH Scotland, U.K.; State Key Laboratory of Heavy Oil Processing, Beijing Key Laboratory of Oil and Gas Pollution Control, College of Chemical Engineering and Environment, China University of Petroleum, Beijing 102249, China;* orcid.org/0000-0001-6874-870X

Complete contact information is available at: https://pubs.acs.org/10.1021/acs.est.1c06596

Notes

The authors declare no competing financial interest.

■ ACKNOWLEDGMENTS

The authors thank Dr. Lina Li for help and support at the BL14W beamline, and Drs. Xiangzhi Zhang, Haigang Liu, Zijian Xu, and Dr. Nian Zhang at the BL08U1 and BL02B02 beamlines in the Shanghai Synchrotron Radiation Facility (SSRF), Shanghai, China, respectively; G.-H.Y. acknowledges research support of the National Key Research and Development Program of China (2020YFC1806803) and the National Natural Science Foundation of China (41977271). A.K. acknowledges the infrastructural support by the DFG under Germany's Excellence Strategy, cluster of Excellence EXC2124, Project ID 390838134. G.M.G. gratefully acknowledges research support of the Geomicrobiology Group from the Natural Environment Research Council, U.K. (NE/M010910/1 and NE/M 011275/1).

■ REFERENCES

(1) Hochella, M. F.; Mogk, D. W.; Ranville, J.; Allen, I. C.; Luther, G. W.; Marr, L. C.; McGrail, B. P.; Murayama, M.; Qafoku, N. P.; Rosso, K. M.; Sahai, N.; Schroeder, P. A.; Vikesland, P.; Westerhoff, P.; Yang, Y. Natural, incidental, and engineered nanomaterials and their impacts on the Earth system. *Science* **2019**, *363*, No. eaau8299.

(2) Smits, M. M.; Herrmann, A. M.; Duane, M.; Duckworth, O. W.; Bonneville, S.; Benning, L. G.; Lundström, U. The fungal−mineral interface: Challenges and considerations of micro-analytical developments. *Fungal Biol. Rev.* **2009**, *23*, 122−131.

(3) Jongmans, A. G.; van Breemen, N.; Lundström, U.; van Hees, P. A. W.; Finlay, R. D.; Srinivasan, M.; Unestam, T.; Giesler, R.; Melkerud, P. A.; Olsson, M. Rock-eating fungi. *Nature* **1997**, *389*, 682−683.

(4) Liang, X.; Hillier, S.; Pendlowski, H.; Gray, N.; Ceci, A.; Gadd, G. M. Uranium phosphate biomineralization by fungi. *Environ. Microbiol.* **2015**, *17*, 2064−2075.

(5) Shah, F.; Nicolás, C.; Bentzer, J.; Ellström, M.; Smits, M.; Rineau, F.; Canbäck, B.; Floudas, D.; Carleer, R.; Lackner, G.; Braesel, J.; Hoffmeister, D.; Henrissat, B.; Ahrén, D.; Johansson, T.; Hibbett, D. S.; Martin, F.; Persson, P.; Tunlid, A. Ectomycorrhizal fungi decompose soil organic matter using oxidative mechanisms adapted from saprotrophic ancestors. *New Phytol.* **2016**, *209*, 1705−1719.

(6) Zhang, J.; Bayram Akcapinar, G.; Atanasova, L.; Rahimi, M. J.; Przylucka, A.; Yang, D.; Kubicek, C. P.; Zhang, R.; Shen, Q.; Druzhinina, I. S. The neutral metallopeptidase NMP1 of *Trichoderma*

guizhouense is required for mycotrophy and self-defence. *Environ. Microbiol.* **2016**, *18*, 580−597.
(7) Yao, S.; Jin, B.; Liu, Z.; Shao, C.; Zhao, R.; Wang, X.; Tang, R. Biomineralization: From material tactics to biological strategy. *Adv. Mater.* **2017**, *29*, No. 1605903.
(8) Liang, K.; Ricco, R.; Doherty, C. M.; Styles, M. J.; Bell, S.; Kirby, N.; Mudie, S.; Haylock, D.; Hill, A. J.; Doonan, C. J.; Falcaro, P. Biomimetic mineralization of metal-organic frameworks as protective coatings for biomacromolecules. *Nat. Commun.* **2015**, *6*, No. 7240.
(9) Aguirre, J.; Ríos-Momberg, M.; Hewitt, D.; Hansberg, W. Reactive oxygen species and development in microbial eukaryotes. *Trends Microbiol.* **2005**, *13*, 111−118.
(10) Hansel, C. M.; Zeiner, C. A.; Santelli, C. M.; Webb, S. M. Mn(II) oxidation by an ascomycete fungus is linked to superoxide production during asexual reproduction. *Proc. Natl. Acad. Sci. U.S.A.* **2012**, *109*, 12621−12625.
(11) Moyo, C. E.; Beckett, R. P.; Trifonova, T. V.; Minibayeva, F. V. Extracellular redox cycling and hydroxyl radical production occurs widely in lichenized Ascomycetes. *Fungal Biol.* **2017**, *121*, 582−588.
(12) Imlay, J. A. Pathways of oxidative damage. *Annu. Rev. Microbiol.* **2003**, *57*, 395−418.
(13) Scott, B.; Eaton, C. J. Role of reactive oxygen species in fungal cellular differentiations. *Curr. Opin. Microbiol.* **2008**, *11*, 488−493.
(14) Selbmann, L.; Egidi, E.; Isola, D.; Onofri, S.; Zucconi, L.; de Hoog, G. S.; Chinaglia, S.; Testa, L.; Tosi, S.; Balestrazzi, A.; Lantieri, A.; Compagno, R.; Tigini, V.; Varese, G. C. Biodiversity, evolution and adaptation of fungi in extreme environments. *Plant Biosyst.* **2013**, *147*, 237−246.
(15) Melton, E. D.; Swanner, E. D.; Behrens, S.; Schmidt, C.; Kappler, A. The interplay of microbially mediated and abiotic reactions in the biogeochemical Fe cycle. *Nat. Rev. Microbiol.* **2014**, *12*, 797−808.
(16) Xu, W.; Jiao, L.; Wu, Y.; Hu, L.; Gu, W.; Zhu, C. Metal−organic frameworks enhance biomimetic cascade catalysis for biosensing. *Adv. Mater.* **2021**, *33*, No. 2005172.
(17) Guo, Z.; Richardson, J. J.; Kong, B.; Liang, K. Nanobiohybrids: Materials approaches for bioaugmentation. *Sci. Adv.* **2020**, *6*, No. eaaz0330.
(18) Wei, H.; Wang, E. Nanomaterials with enzyme-like characteristics (nanozymes): Next-generation artificial enzymes. *Chem. Soc. Rev.* **2013**, *42*, 6060−6093.
(19) Aleklett, K.; Boddy, L. Fungal behaviour: A new frontier in behavioural ecology. *Trend. Ecol. Evol.* **2021**, *36*, 787−796.
(20) Navrotsky, A.; Mazeina, L.; Majzlan, J. Size-driven structural and thermodynamic complexity in iron oxides. *Science* **2008**, *319*, 1635−1638.
(21) Kleber, M.; Bourg, I. C.; Coward, E. K.; Hansel, C. M.; Myneni, S. C. B.; Nunan, N. Dynamic interactions at the mineral−organic matter interface. *Nat. Rev. Earth Environ.* **2021**, *2*, 402−421.
(22) Gao, L.; Zhuang, J.; Nie, L.; Zhang, J.; Zhang, Y.; Gu, N.; Wang, T.; Feng, J.; Yang, D.; Perrett, S.; Yan, X. Intrinsic peroxidase-like activity of ferromagnetic nanoparticles. *Nat. Nanotechnol.* **2007**, *2*, 577−583.
(23) Chen, Z.; Yin, J.-J.; Zhou, Y.-T.; Zhang, Y.; Song, L.; Song, M.; Hu, S.; Gu, N. Dual enzyme-like activities of iron oxide nanoparticles and their implication for diminishing cytotoxicity. *ACS Nano* **2012**, *6*, 4001−4012.
(24) Huang, Y.; Ren, J.; Qu, X. Nanozymes: Classification, catalytic mechanisms, activity regulation, and applications. *Chem. Rev.* **2019**, *119*, 4357−4412.
(25) Wang, X.; Gao, X. J.; Qin, L.; Wang, C.; Song, L.; Zhou, Y.-N.; Zhu, G.; Cao, W.; Lin, S.; Zhou, L.; Wang, K.; Zhang, H.; Jin, Z.; Wang, P.; Gao, X.; Wei, H. e_g occupancy as an effective descriptor for the catalytic activity of perovskite oxide-based peroxidase mimics. *Nat. Commun.* **2019**, *10*, No. 704.
(26) Yu, G.-H.; Chi, Z.-L.; Kappler, A.; Sun, F.-S.; Liu, C.-Q.; Teng, H. H.; Gadd, G. M. Fungal nanophase particles catalyze iron transformation for oxidative stress removal and iron acquisition. *Curr. Biol.* **2020**, *30*, 2943−2950.
(27) Chi, Z.-L.; Zhao, X.-Y.; Chen, Y.-L.; Hao, J.-L.; Yu, G.-H.; Goodman, B. A.; Gadd, G. M. Intrinsic enzyme-like activity of magnetite particles is enhanced by cultivation with *Trichoderma guizhouense*. *Environ. Microbiol.* **2021**, *23*, 893−907.
(28) Voinov, M. A.; Pagán, J. O. S.; Morrison, E.; Smirnova, T. I.; Smirnov, A. I. Surface-mediated production of hydroxyl radicals as a mechanism of iron oxide nanoparticle biotoxicity. *J. Am. Chem. Soc.* **2011**, *133*, 35−41.
(29) Huang, X.; Hou, X.; Zhao, J.; Zhang, L. Hematite facet confined ferrous ions as high efficient Fenton catalysts to degrade organic contaminants by lowering H_2O_2 decomposition energetic span. *Appl. Catal., B* **2016**, *181*, 127−137.
(30) Bonneville, S.; Delpomdor, F.; Préat, A.; Chevalier, C.; Araki, T.; Kazemian, M.; Steele, A.; Schreiber, A.; Wirth, R.; Benning, L. G. Molecular identification of fungi microfossils in a Neoproterozoic shale rock. *Sci. Adv.* **2020**, *6*, No. eaax7599.
(31) Youn, W.; Kim, J. Y.; Park, J.; Kim, N.; Choi, H.; Cho, H.; Choi, I. S. Single-cell nanoencapsulation: From passive to active shells. *Adv. Mater.* **2020**, *32*, No. 1907001.
(32) Harman, G. E.; Howell, C. R.; Viterbo, A.; Chet, I.; Lorito, M. *Trichoderma* species — opportunistic, avirulent plant symbionts. *Nat. Rev. Microbiol.* **2004**, *2*, 43−56.
(33) Gao, Q.-X.; Wang, X.-F.; Di, J.-L.; Wu, X.-C.; Tao, Y.-R. Enhanced catalytic activity of α-Fe_2O_3 nanorods enclosed with {110} and {001} planes for methane combustion and CO oxidation. *Catal. Sci. Technol.* **2011**, *1*, 574−577.
(34) Cao, F.; Zhang, L.; Wang, H.; You, Y.; Wang, Y.; Gao, N.; Ren, J.; Qu, X. Defect-rich adhesive nanozymes as efficient antibiotics for enhanced bacterial inhibition. *Angew. Chem., Int. Ed.* **2019**, *58*, 16236−16242.
(35) Dissegna, S.; Epp, K.; Heinz, W. R.; Kieslich, G.; Fischer, R. A. Defective metal-organic frameworks. *Adv. Mater.* **2018**, *30*, No. 1704501.
(36) Jiang, B.; Duan, D.; Gao, L.; Zhou, M.; Fan, K.; Tang, Y.; Xi, J.; Bi, Y.; Tong, Z.; Gao, G. F.; Xie, N.; Tang, A.; Nie, G.; Liang, M.; Yan, X. Standardized assays for determining the catalytic activity and kinetics of peroxidase-like nanozymes. *Nat. Protoc.* **2018**, *13*, 1506−1520.
(37) Schwertmann, U.; Cornell, R. M. *Iron Oxides in the Laboratory: Preparation and Characterization*; John Wiley & Sons, 2008; pp 103−112.
(38) McCafferty, E.; Wightman, J. P. Determination of the concentration of surface hydroxyl groups on metal oxide films by a quantitative XPS method. *Surf. Interface Anal.* **1998**, *26*, 549−564.
(39) Posth, N. R.; Canfield, D. E.; Kappler, A. Biogenic Fe(III) minerals: From formation to diagenesis and preservation in the rock record. *Earth-Sci. Rev.* **2014**, *135*, 103−121.
(40) Yu, G.-H.; Chi, Z.-L.; Henry Teng, H.; Dong, H.-L.; Kappler, A.; Gillings, M. R.; Polizzotto, M. L.; Liu, C.-Q.; Zhu, Y.-G. Fungus-initiated catalytic reactions at hyphal-mineral interfaces drive iron redox cycling and biomineralization. *Geochim. Cosmochim. Acta* **2019**, *260*, 192−203.
(41) Parlanti, E.; Wörz, K.; Geoffroy, L.; Lamotte, M. Dissolved organic matter fluorescence spectroscopy as a tool to estimate biological activity in a coastal zone submitted to anthropogenic inputs. *Org. Geochem.* **2000**, *31*, 1765−1781.
(42) Voinov, M. A.; Pagán, J. O. S.; Morrison, E.; Smirnova, T. I.; Smirnov, A. I. Surface-mediated production of hydroxyl radicals as a mechanism of iron oxide nanoparticle biotoxicity. *J. Am. Chem. Soc.* **2011**, *133*, 35−41.
(43) Mueller, D. N.; Machala, M. L.; Bluhm, H.; Chueh, W. C. Redox activity of surface oxygen anions in oxygen-deficient perovskite oxides during electrochemical reactions. *Nat. Commun.* **2015**, *6*, No. 6097.
(44) Li, Y.; Li, Y.; Xu, X.; Ding, C.; Chen, N.; Ding, H.; Lu, A. Structural disorder controlled oxygen vacancy and photocatalytic activity of spinel-type minerals: A case study of $ZnFe_2O_4$. *Chem. Geol.* **2019**, *504*, 276−287.

https://doi.org/10.1021/acs.est.1c06596
Environ. Sci. Technol. 2022, 56, 672−680

(45) Li, M.; Deng, J.; Pu, A.; Zhang, P.; Zhang, H.; Gao, J.; Hao, Y.; Zhong, J.; Sun, X. Hydrogen-treated hematite nanostructures with low onset potential for highly efficient solar water oxidation. *J. Mater. Chem. A* **2014**, *2*, 6727−6733.
(46) Zhang, Z.; Karimata, I.; Nagashima, H.; Muto, S.; Ohara, K.; Sugimoto, K.; Tachikawa, T. Interfacial oxygen vacancies yielding long-lived holes in hematite mesocrystal-based photoanodes. *Nat. Commun.* **2019**, *10*, No. 4832.
(47) Diaz, J. M.; Plummer, S.; Hansel, C. M.; Andeer, P. F.; Saito, M. A.; McIlvin, M. R. NADPH-dependent extracellular superoxide production is vital to photophysiology in the marine diatom *Thalassiosira oceanica*. *Proc. Natl. Acad. Sci. U.S.A.* **2019**, *116*, 16448−16453.
(48) Winterbourn, C. C. Reconciling the chemistry and biology of reactive oxygen species. *Nat. Chem. Biol.* **2008**, *4*, 278−286.
(49) Chadwick, G. L.; Jiménez Otero, F.; Gralnick, J. A.; Bond, D. R.; Orphan, V. J. NanoSIMS imaging reveals metabolic stratification within current-producing biofilms. *Proc. Natl. Acad. Sci. U.S.A.* **2019**, *116*, 20716−20724.
(50) Liang, K.; Richardson, J. J.; Cui, J.; Caruso, F.; Doonan, C. J.; Falcaro, P. Metal−organic framework coatings as cytoprotective exoskeletons for living cells. *Adv. Mater.* **2016**, *28*, 7910−7914.
(51) Park, J. H.; Hong, D.; Lee, J.; Choi, I. S. Cell-in-shell hybrids: Chemical nanoencapsulation of individual cells. *Acc. Chem. Res.* **2016**, *49*, 792−800.
(52) Ji, Z.; Zhang, H.; Liu, H.; Yaghi, O. M.; Yang, P. Cytoprotective metal-organic frameworks for anaerobic bacteria. *Proc. Natl. Acad. Sci. U.S.A.* **2018**, *115*, 10582−10587.
(53) Xiao, J.; He, X. H.; Hao, J. L.; Zhou, Y.; Zheng, L. Y.; Ran, W.; Shen, Q. R.; Yu, G. H. New strategies for submicron characterization the carbon binding of reactive minerals in long-term contrasting fertilized soils: Implications for soil carbon storage. *Biogeosciences* **2016**, *13*, 3607−3618.
(54) Yang, S. H.; Kang, S. M.; Lee, K.-B.; Chung, T. D.; Lee, H.; Choi, I. S. Mussel-inspired encapsulation and functionalization of individual yeast cells. *J. Am. Chem. Soc.* **2011**, *133*, 2795−2797.
(55) Sugunan, A.; Melin, P.; Schnürer, J.; Hilborn, J. G.; Dutta, J. Nutrition-driven assembly of colloidal nanoparticles: Growing fungi assemble gold nanoparticles as microwires. *Adv. Mater.* **2007**, *19*, 77−81.
(56) Garrido-Ramírez, E. G.; Theng, B. K. G.; Mora, M. L. Clays and oxide minerals as catalysts and nanocatalysts in Fenton-like reactions — A review. *Appl. Clay Sci.* **2010**, *47*, 182−192.
(57) Herget, K.; Hubach, P.; Pusch, S.; Deglmann, P.; Götz, H.; Gorelik, T. E.; Gural'skiy, I. yA.; Pfitzner, F.; Link, T.; Schenk, S.; Panthöfer, M.; Ksenofontov, V.; Kolb, U.; Opatz, T.; André, R.; Tremel, W. Haloperoxidase mimicry by CeO_{2-x} nanorods combats biofouling. *Adv. Mater.* **2017**, *29*, No. 1603823.
(58) Wang, Z.; Mao, X.; Chen, P.; Xiao, M.; Monny, S. A.; Wang, S.; Konarova, M.; Du, A.; Wang, L. Understanding the roles of oxygen vacancies in hematite-based photoelectrochemical processes. *Angew. Chem., Int. Ed.* **2019**, *58*, 1030−1034.
(59) Xu, S.; Zheng, H.; Ma, R.; Wu, D.; Pan, Y.; Yin, C.; Gao, M.; Wang, W.; Li, W.; Liu, S.; Chai, Z.; Li, R. Vacancies on 2D transition metal dichalcogenides elicit ferroptotic cell death. *Nat. Commun.* **2020**, *11*, No. 3484.
(60) Cai, X.; Dong, J.; Liu, J.; Zheng, H.; Kaweeteerawat, C.; Wang, F.; Ji, Z.; Li, R. Multi-hierarchical profiling the structure-activity relationships of engineered nanomaterials at nano-bio interfaces. *Nat. Commun.* **2018**, *9*, No. 4416.
(61) Yu, G.-H.; Kuzyakov, Y.; Luo, Y.; Goodman, B.; Kappler, A.; Liu, F.-F.; Sun, F.-S. Molybdenum bioavailability and asymbiotic nitrogen fixation in soil are raised by iron (oxyhydr)oxide mediated free radical production. *Environ. Sci. Technol.* **2021**, *55*, 14979−14989.
(62) Op De Beeck, M.; Troein, C.; Peterson, C.; Persson, P.; Tunlid, A. Fenton reaction facilitates organic nitrogen acquisition by an ectomycorrhizal fungus. *New Phytol.* **2018**, *218*, 335−343.
(63) Yu, G.-H.; Kuzyakov, Y. Fenton chemistry and reactive oxygen species in soil: Abiotic mechanisms of biotic processes, controls and consequences for carbon and nutrient cycling. *Earth-Sci. Rev.* **2021**, *214*, No. 103525.
(64) Chi, Z.-L.; Yu, G.-H. Nanozyme-mediated elemental biogeochemical cycling and environmental effects. *Sci. China Earth Sci.* **2021**, *64*, 1015−1025.
(65) Gleason, F. H.; Larkum, A. W. D.; Raven, J. A.; Manohar, C. S.; Lilje, O. Ecological implications of recently discovered and poorly studied sources of energy for the growth of true fungi especially in extreme environments. *Fungal Ecol.* **2019**, *39*, 380−387.
(66) Huang, S.; Kou, X.; Shen, J.; Chen, G.; Ouyang, G. "Armor-plating" enzymes with metal−organic frameworks (MOFs). *Angew. Chem., Int. Ed.* **2020**, *59*, 8786−8798.
(67) Park, J. H.; Yang, S. H.; Lee, J.; Ko, E. H.; Hong, D.; Choi, I. S. Nanocoating of single cells: From maintenance of cell viability to manipulation of cellular activities. *Adv. Mater.* **2014**, *26*, 2001−2010.
(68) Wang, R.; Li, H.; Sun, J.; Zhang, L.; Jiao, J.; Wang, Q.; Liu, S. Nanomaterials facilitating microbial extracellular electron transfer at interfaces. *Adv. Mater.* **2021**, *33*, No. 2004051.
(69) Shi, L.; Dong, H.; Reguera, G.; Beyenal, H.; Lu, A.; Liu, J.; Yu, H.-Q.; Fredrickson, J. K. Extracellular electron transfer mechanisms between microorganisms and minerals. *Nat. Rev. Microbiol.* **2016**, *14*, 651−662.
(70) Loron, C. C.; François, C.; Rainbird, R. H.; Turner, E. C.; Borensztajn, S.; Javaux, E. J. Early fungi from the Proterozoic era in Arctic Canada. *Nature* **2019**, *570*, 232−235.
(71) Malhi, Y. The Concept of the Anthropocene. *Annu. Rev. Environ. Resour.* **2017**, *42*, 77−104.
(72) Bar-On, Y. M.; Phillips, R.; Milo, R. The biomass distribution on Earth. *Proc. Natl. Acad. Sci. U.S.A.* **2018**, *115*, 6506−6511.
(73) He, L.; Mazza Rodrigues, J. L.; Soudzilovskaia, N. A.; Barceló, M.; Olsson, P. A.; Song, C.; Tedersoo, L.; Yuan, F.; Yuan, F.; Lipson, D. A.; Xu, X. Global biogeography of fungal and bacterial biomass carbon in topsoil. *Soil Biol. Biochem.* **2020**, *151*, No. 108024.
(74) Schaefer, C. E.; Ho, P.; Berns, E.; Werth, C. Mechanisms for abiotic dechlorination of trichloroethene by ferrous minerals under oxic and anoxic conditions in natural sediments. *Environ. Sci. Technol.* **2018**, *52*, 13747−13755.

https://doi.org/10.1021/acs.est.1c06596
Environ. Sci. Technol. 2022, 56, 672−680